Dark interlayer plasmons in colloidal gold nanoparticle bi- and fewlayers

Niclas S. Mueller,[*,†,‖] Bruno G. M. Vieira,[†,‡,‖] Florian Schulz,[¶] Patryk Kusch,[†] Valerio Oddone,[†] Eduardo B. Barros,[‡] Holger Lange,[¶,§] and Stephanie Reich[*,†]

†*Freie Universität Berlin, Department of Physics, Arnimallee 14, D-14195 Berlin, Germany*

‡*Departamento de Física, Universidade Federal do Ceará, Fortaleza, Brazil*

¶*University of Hamburg, Institute for Physical Chemistry, Martin-Luther-King Platz 6, 20146 Hamburg, Germany*

§*The Hamburg Centre for Ultrafast Imaging, 22761 Hamburg, Germany*

‖*Contributed equally to this work*

E-mail: niclasm@physik.fu-berlin.de; reich@physik.fu-berlin.de

Abstract

We demonstrate the excitation of dark plasmon modes with linearly polarized light at normal incidence in self-assembled layers of gold nanoparticles. Because of field retardation the incident light field induces plasmonic dipoles that are parallel within each layer but antiparallel between the layers resulting in a vanishing net dipole moment. Using micro-absorbance spectroscopy we measured a pronounced absorbance peak and reflectance dip at 1.5 eV for bi- and trilayers of gold nanoparticles with a diameter of 46 nm and 2 nm interparticle gap size. The excitation was identified as the dark interlayer plasmon by finite-difference time-domain simulations. The dark plasmon modes are predicted to evolve into standing waves when further increasing the layer

number which leads to 90% transmittance of the incident light through the nanoparticle film. Our approach is easy to implement and paves the way for large-area coatings with tunable plasmon resonance.

Keywords

dark plasmon, self-assembly, gold nanoparticles, bilayer, micro-absorbance spectroscopy, finite-difference time-domain (FDTD)

Noble metal nanoparticles strongly interact with light because of the collective excitation of free electrons, which is known as a localized surface plasmon resonance (LSPR).[1,2] Plasmon resonances offer the possibility to manipulate light on the nanoscale, which enables nanophotonic components, novel light sources and improved photovoltaic devices.[3–5] The intense electric fields in the vicinity of the metal surface are exploited to enhance optical processes, giving rise to phenomena like surface-enhanced Raman scattering and surface-enhanced infrared absorption.[6–9] The efficient interaction with far-field radiation, on the other hand, leads to a radiative plasmon decay within a few femtoseconds.[2,10] This radiative damping is a drawback for applications that require high quality factors, such as chemical or biological sensors.[11]

Dark plasmon modes received considerable attention in the past years because they exhibit a vanishing dipole moment and do not suffer from radiative losses.[12–23] Such modes can be either multipolar modes in individual nanoparticles or a hybridization of dipole modes in coupled nanoparticles with a vanishing total dipole moment.[24,25] Various techniques were proposed to excite dark plasmons: Dark modes were partially turned bright by making plasmonic nanostructures asymmetric and thereby introducing a non-zero net dipole moment.[13–15] The evanescent fields of local emitters and wave guides as well as magnetic fields were used for the excitation.[16–19] It was proposed to excite dark modes in plasmonic oligomers with radial and azimuthal polarization and multipolar modes in single nanoparticles with optical vortex beams.[20–22] Finally, bright plasmon modes may couple to dark plasmon modes, which gives rise to Fano resonances and a plasmonic analogue to electromagnetically induced transparency.[23] All these approaches have in common that either complex plasmonic nanostructures need to be produced by demanding techniques such as electron-beam lithography or specific light sources are required for excitation. This is a great challenge for the systematic optimization of dark modes, their low-cost applications, and scalability.

Here we demonstrate the excitation of dark plasmons in colloidal layers of gold nanoparticles by linearly-polarized light at normal incidence. Because of field retardation the incident

light field induces dipoles that are antiparallel in the layers exciting dark interlayer plasmons that are strongly red shifted (∼800 meV) compared to the bright plasmon in a monolayer. Using micro-absorbance measurements and finite-difference time-domain (FDTD) simulations we confirm the excitation of the dark modes in self-assembled bi- and trilayers of gold nanoparticles with an absorption intensity of up to 50%. When further increasing the layer number, the dark modes transform into standing waves that transmit the light through the nanoparticle film.

Results and discussion

To introduce our concept for the excitation of a dark interlayer plasmon, we first consider a gold nanoparticle dimer. Fig. 1a displays the plasmonic modes of the dimer that arise from the hybridization of the dipolar modes of the individual particles.[26] There are two bright modes of dipolar character. They belong to the B_{3u} representation of the D_{2h} point group if the dipoles in the two particles are parallel and along the dimer axis (x axis) and to the B_{2u} representation for parallel dipoles along y.[27] Furthermore, there are two dark modes with antiparallel dipole moments in both particles. They belong to the A_{1g} representation for dipoles along the x axis and to the B_{1g} representation for dipoles along y. The eigenenergies of the B_{3u} and B_{1g} modes are red shifted compared to the plasmon of the single particle because the modes are of binding character. The B_{2u} and A_{1g} modes are blue shifted because they are antibinding.

The bright modes can be excited by a plane electromagnetic wave with wave vector perpendicular to the dimer axis, as can be seen from the calculated absorption cross sections in Fig. 1b. The $B_{3u}(x)$ mode (1.66 eV, orange curve) is excited for light polarization along the x axis and the $B_{2u}(y)$ mode for polarization along y (1.88 eV, blue curve). The dark modes are usually inaccessible with far field radiation because of their vanishing net dipole moment. However, from the absorption cross section in Fig. 1b it is apparent that the

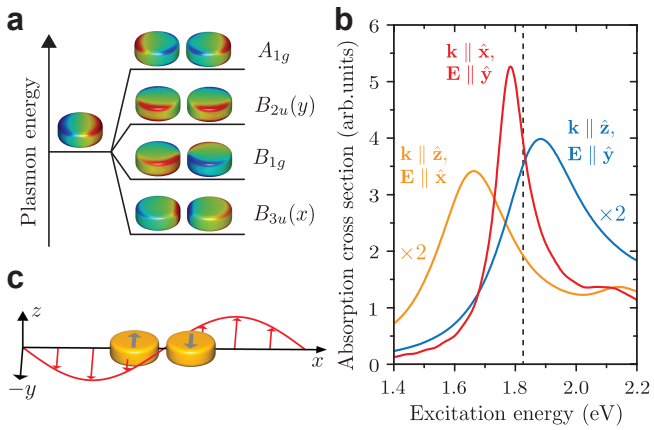

Figure 1: Excitation of a dark plasmon in a gold nanoparticle dimer by side illumination. (a) Hybridization diagram for the plasmon modes of a dimer that belong to a combination of plasmonic dipoles in both particles. The surface charges (red - positive, blue - negative) were calculated with the boundary-elements method.[28] (b) Absorption cross section simulated with the FDTD method for different directions and polarizations of an incoming plane wave (100 nm disk diameter, 20 nm disk height, 20 nm gap between disks, background index $n = 1.33$). The absorption maximum of the dipole mode of a single particle is indicated by a dashed line. (c) Sketch illustrating the excitation of the dark B_{1g} mode by light that is incident along the dimer axis. The gray arrows show the dipole moments excited in both disks.

dark B_{1g} mode (1.78 eV, red curve) is excited by illuminating the dimer from the side, as illustrated in Fig. 1c. The spectral width of the dark plasmon peak is with 150 meV by a factor of two narrower than that of the bright plasmon modes, which shows that radiative damping is suppressed.

The activation of the dark plasmon is explained by the retardation of the incident light field (Fig. 1c).[18,29] For certain times the electric field vectors (red arrows) are antiparallel at the two disks and therefore excite antiparallel dipole moments in both particles (gray arrows). The effect is most pronounced when the center-to-center distance of the two disks equals half of the light wavelength. We note that symmetry-derived selection rules fail to predict the excitation of the dark plasmon, because the analysis assumes the light wavelength to be much larger than the system size. While this is certainly correct for molecules and crystal unit cells, the approximation breaks down for extended nanostructures like the plasmonic dimer considered here. A careful choice of nanostructure geometry and experimental conditions

may allow the observation of excitations that are generally considered to be forbidden by selection rules.

Remarkably, the absorption peak of the bright $B_{2u}(y)$ mode at 1.88 eV is missing for the side illumination geometry, although the simulation was carried out for a dimer with a center-to-center distance of 120 nm $\approx \lambda/4$. The maximum absorption cross section of the dark mode is by a factor of three stronger than absorption by the bright modes. The optical absorption by the dark plasmon is dominant as long as the dimer is large enough that field retardation is important. For a much smaller dimer with a center-to-center distance of 24 nm, the absorption spectrum is dominated by the $B_{2u}(y)$ mode and the dark mode is not excited (see Fig. S1 in the Supporting Information).

Realizing the scattering geometry of Fig. 1c experimentally requires incident light parallel to the substrate or stacking two nanoparticles on top of each other. The latter has been realized with metal-insulator-metal nanodisks, where the antisymmetric dark mode was activated by an asymmetry of the two metal disks and field retardation.[19,29–32] We now demonstrate the excitation of an equivalent dark mode in colloidal nanoparticle bilayers. This approach benefits from its scalability, and can be extended to multiple stacked nanoparticle layers. Furthermore, small gap sizes of a few nm are naturally realized and lead to strongly coupled plasmonic modes.

Fig. 2 shows the simulated absorbance and reflectance of hexagonally close-packed (hcp) mono- and bilayers of spherical gold nanoparticles. The nanoparticle layers are illuminated with linearly polarized light at normal incidence (Fig. 2a and b). For a monolayer of gold nanoparticles the absorbance spectrum is dominated by gold interband transitions that set in at 2 eV.[2,33] A weak peak at 2.25 eV stems from a bright plasmon in which all dipoles are parallel (white arrows in Fig. 2a).

The spectrum changes dramatically for a bilayer of gold nanoparticles (Fig. 2d). A pronounced absorbance peak appears in the spectrum at 1.44 eV, which is absent for the monolayer. To identify the plasmon mode we extract the sign and magnitude of the electrical

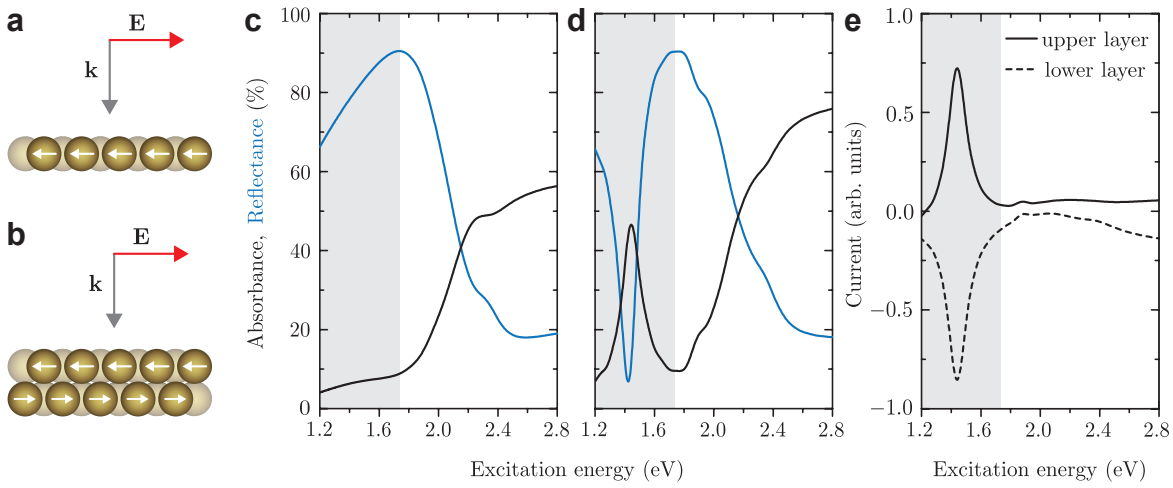

Figure 2: Optical response of colloidal gold nanosphere mono- and bilayers simulated by FDTD. (a) Sketch illustrating the excitation of a bright dipole plasmon in a nanoparticle monolayer by normal incidence of linearly polarized light with wave vector **k** and polarization **E**. The plasmonic dipole moments are indicated by white arrows. (b) Sketch illustrating the excitation of a dark interlayer plasmon in a nanoparticle bilayer. (c) Absorbance and reflectance spectra of a monolayer and (d) a bilayer of gold nanospheres (diameter $d = 46$ nm) that are hexagonally close packed with gaps of 2 nm. The background medium has a refractive index of $n = 1.4$. The spectral range that is relevant for the excitation of the dark interlayer plasmon is shaded gray. (e) Magnitude of the electrical current in the nanoparticles of the bilayer as a function of excitation energy. The component that is parallel to the polarization **E** is plotted at a phase shift of $3\pi/2$ to the incident light field.

current in both nanoparticle layers from the FDTD simulations (Fig. 2e). The current in both layers contains a peak at the same excitation energy as the absorbance and remains close to zero for all other excitation energies. The current flows in opposite directions in the two nanoparticle layers (compare solid and dashed curves in Fig. 2e). This clearly shows that the plasmon mode corresponds to a hybridization of antiparallel dipole moments in the two layers as shown by the white arrows in Fig. 2b. Because of the vanishing net dipole moment this is a dark plasmon, similar to the B_{1g} mode of the nanoparticle dimer.

The resonance energy 1.44 eV of the antiparallel dark mode is strongly red shifted from the bright plasmon in a monolayer at 2.25 eV because of the bonding interaction between the two layers. We also note that the reduced radiative damping of the dark plasmon leads to a FWHM of 180 meV that is by a factor of three smaller than for the bright excitation

as we calculated with a silver structure (Fig. S2). In the case of gold the bright plasmon is no longer visible in the bilayer spectrum, Fig. 2d, because damping by interband transitions is much stronger than for the monolayer due to the blueshift of the antibonding layer-layer mode.

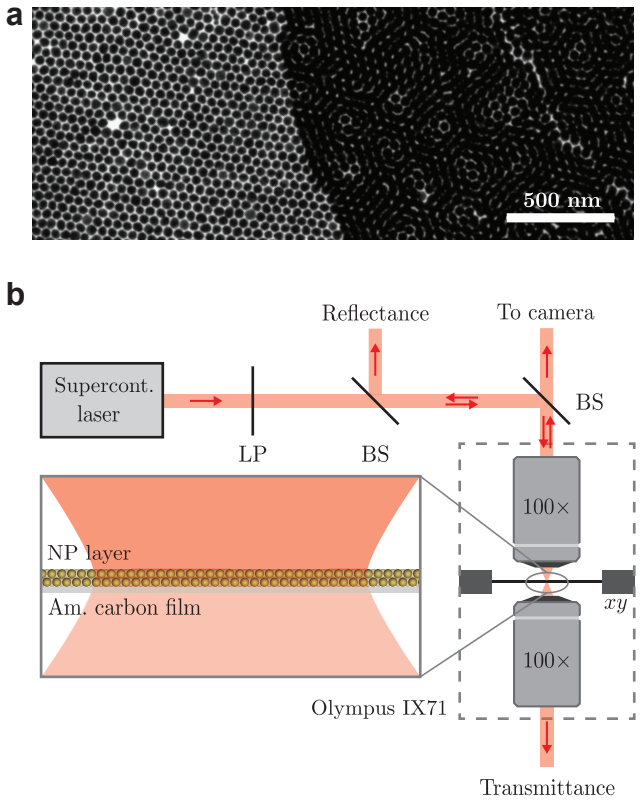

Figure 3: (a) Transmission electron microscopy (TEM) image of a colloidal gold nanoparticle monolayer (left) and bilayer (right). A Moiré pattern indicates a small twist angle between the two layers. (b) Experimental set-up for the micro-absorbance measurements. The light of a supercontinuum laser (red) passes through a linear polarizer (LP) and is guided into an inverted microscope (dashed box). The laser beam is focused by an objective onto the gold nanoparticle film on the TEM grid; see sketch in the inset. The TEM grid is mounted on a motorized xy translation stage. The transmitted light is collected by a second objective and coupled into a fiber that is connected to a spectrometer. The reflected light is guided by beam splitters (BS) to a microscope camera and via a fiber to a spectrometer. The light propagation direction is indicated by red arrows.

We now turn to an experimental verification of the suggested theoretical concept using self-assembled gold nanoparticle films. Fig. 3a shows a monolayer of hexagonally close-packed nanoparticles on the left and a bilayer to the right. The Moiré pattern indicates that the two

layers overlap with a small twist angle. From TEM images we deduced a particle diameter of 46±3 nm and an average interparticle gap size of ∼2 nm. To measure the absorbance of the nanoparticle layers, we used a home-built micro-absorbance spectrometer (Fig. 3b). The set-up was integrated into an optical microscope which enabled us to simultaneously measure reflectance and transmittance at specific positions that were imaged with a TEM afterwards.

We measured the transmittance and reflectance at numerous mono- and bilayers of gold nanoparticles on different TEM grids and obtained reproducibly the same spectra. In Fig. 4, we plot the reflectance and absorbance spectra of two places. The corresponding transmittance spectra and TEM images of the two places are given in Figs. S3-S5 in the Supporting Information. The spectra of a monolayer in Fig. 4a nicely resemble the simulated spectra in Fig. 2c. The absorption edge sets in for excitation energies larger than 2 eV, which is attributed to interband transitions.[2,33] A peak from the bright plasmon is hardly visible at 2.25 eV. The spectra of the nanoparticle bilayers are dominated by a pronounced reflectance dip at 1.48 eV and an absorbance peak at 1.53 eV (see Figs. 4b and c, gray shaded area) in excellent agreement with the predictions. From a comparison to the simulated spectra in Fig. 2 the absorbance peak is unambiguously assigned to the excitation of the dark interlayer plasmon mode.

The absorbance peaks and reflectance dips in Figs. 4b and c are with a FWHM of ∼ 360 meV by a factor of two broader than in the simulated spectra in Fig. 2d. We attribute this to variations of the nanoparticle size and gaps as visible in the TEM images; see Fig. 3a and images with higher magnification in the Supporting Information. We found by FDTD simulations that the gap size between the nanoparticles within the two layers strongly affects the spectral position of the absorbance peak. An increase in gap size of 0.5 nm blue shifts the peak by 70 meV (Fig. S6). Taking this into account we averaged the simulated spectra with varying gap size, Fig. 4d, and obtained excellent agreement with experiment. This shows that the width in the experimental spectra is given by inhomogeneous broadening

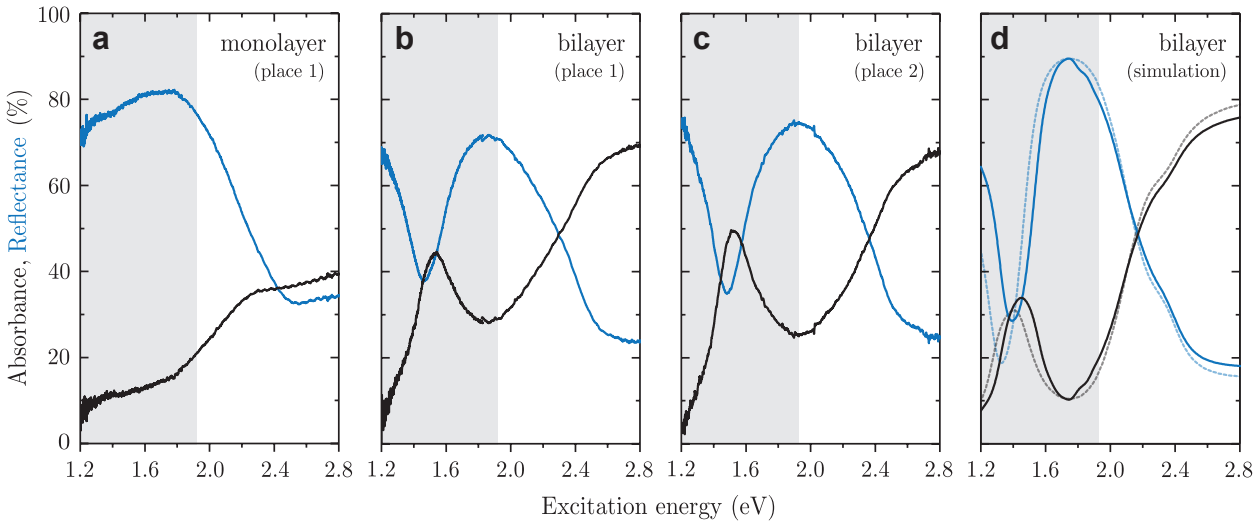

Figure 4: Micro-absorbance and reflectance spectra of (a) a colloidal gold nanoparticle monolayer and (b) and (c) gold nanoparticle bilayers. A pronounced absorbance peak and reflectance dip is visible in the near infrared in the spectra of the bilayers and absent in the spectra of the monolayer (gray shaded area). This peak is attributed to the excitation of a dark interlayer plasmon. (d) FDTD simulation of the reflectance and absorbance of a gold nanoparticle bilayer calculated as the average of the spectra for three gap sizes of 1.5 nm, 2 nm and 2.5 nm. All other parameters are similar to those in Fig. 2. The dotted lines are simulated spectra for the stacking where the nanoparticle layers are aligned.

due to a dispersion in gap size and not the radiative decay rate. We did not observe any further broadening of the line width when measuring with laser spot sizes much larger than the diffraction limit, i.e. using a 20× objective with a numerical aperture of 0.25 (Fig. S7). The variations in interparticle gap sizes therefore occur on length scales smaller than the wavelength of the incident light. Since the interparticle distance can be experimentally adjusted during synthesis, it offers the possibility to tune the spectral position of the plasmonic resonance.[34]

The TEM images in Figs. 3a, S4a and S5a show that the two nanoparticle layers do not align hexagonally close-packed (hcp) as was assumed in the simulations but with a varying twist angle. To test the role of stacking, we simulated the absorbance and reflectance spectra for two gold nanoparticle layers that are aligned on top of each other (dotted lines in Fig. 4d). The absorbance peak of the dark plasmon is red shifted by 50 meV compared to the spectral position for hcp stacking. Besides the small shift, the spectral features in the

absorbance and reflectance spectra remain unchanged. We conclude that the exact stacking is negligible for the spectral position and intensity of the dark mode. Close-packed layers of gold nanoparticles can be synthesized with grain sizes of several hundreds of μm^2.[35] Stacking two monolayers will enable large-area coatings with tunable plasmonic resonances.

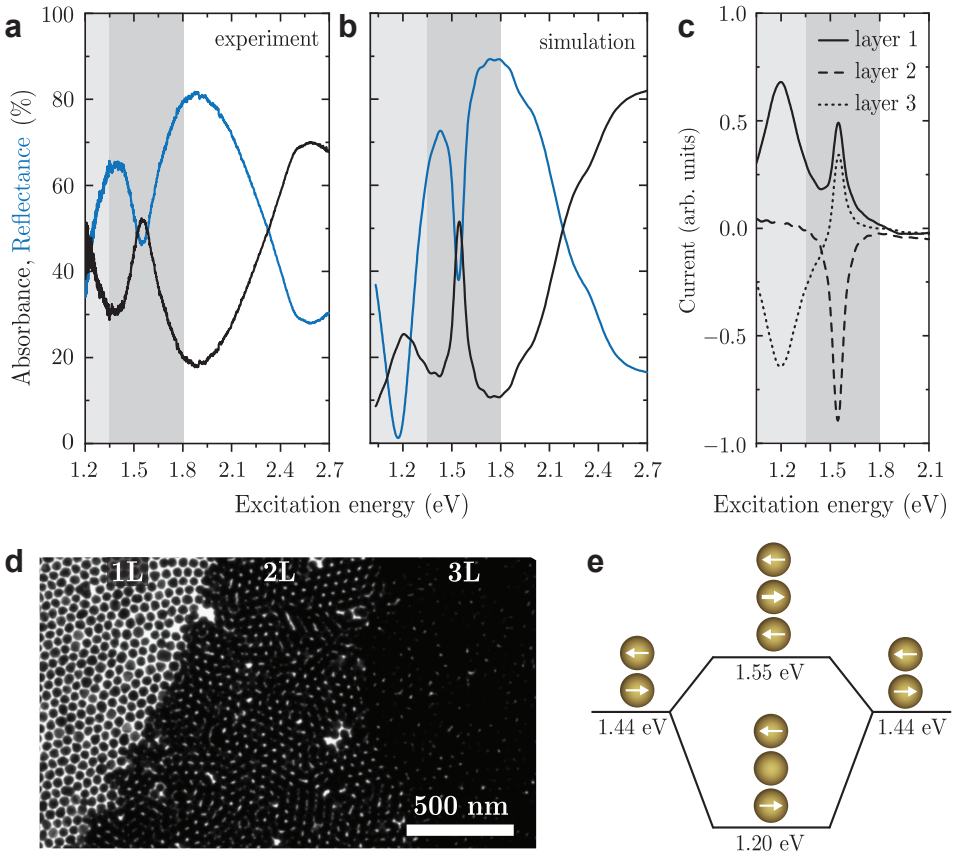

Figure 5: Excitation of a dark plasmon in a gold nanoparticle trilayer. (a) Experimental micro-absorbance and reflectance spectra. (b) Simulated absorbance and reflectance with FDTD for a trilayer with hcp stacking, 46 nm sphere diameter, gaps of 2 nm and a background medium with a refractive index of $n = 1.4$. (c) Magnitude of the electrical current in the three layers as a function of excitation energy. The component that is parallel to the polarization $\mathbf{E}$ is plotted at a phase shift of $3\pi/2$ to the incident light field. Layer 1 faces the incident light. (d) TEM image showing a gold nanoparticle monolayer (1L), bilayer (2L) and the trilayer (3L) where the spectra were recorded. (e) Hybridization diagram of the dark modes in the nanoparticle trilayer by a symmetric and antisymmetric combination of the dark mode in the bilayer. The mode at 1.55 eV is shaded dark gray and the mode at 1.20 eV light gray in the spectra.

Finally, we demonstrate that the concept of dark mode excitation in a nanoparticle bilayer can be extended to more than two layers giving rise to a rich variety of dark interlayer

plasmons. In Fig. 5a we show the absorbance and reflectance spectrum measured on a nanoparticle trilayer. Similar to the bilayer the spectrum is dominated by a pronounced absorbance peak at 1.57 eV which is with a FWHM of 220 meV, 40% narrower than for the bilayer. The onset of a second peak below 1.2 eV is visible, which is outside our measurement range. The two peaks are clearly identified from a simulated spectrum for a trilayer of hcp stacked gold nanoparticles (Fig. 5b). From the electrical current distribution inside the nanoparticles, Fig. 5c, the two peaks are both assigned to dark interlayer plasmons with a vanishing net dipole moment. The two modes can be explained by a symmetric (1.2 eV) and antisymmetric (1.55 eV) hybridization of the dark bilayer mode at 1.44 eV (Fig. 5e). The peak at 1.2 eV is the analog to the dark interlayer plasmon of the bilayer, where the dipoles in the nanoparticles of the outer layers are antiparallel. The plasmon resonance at 1.55 eV corresponds to antiparallel dipoles in all neighboring layers. It has a simulated FWHM of only 80 meV which corresponds to a Q factor of $Q = \omega/\Delta\omega = 19.4$. Its activation may be explained by a coupling to the magnetic component of the incident light field, similar to transverse magnetic modes in metal-insulator-metal stacks.[18,36]

The trend of activating additional dark interlayer plasmons continues when further increasing the layer number. In Fig. 6a we plot the simulated absorbance spectra for two to five hcp stacked gold nanoparticle layers. With each additional layer a new peak appears in the spectrum, which corresponds to a mode where the plasmonic dipoles in all neighboring layers are antiparallel (Fig. 6a, inset and Fig. S9). All other peaks are red shifted and broadened upon increasing the layer number. The electrical currents in the top and bottom layers always have the same magnitude.

The absorbance of the lowest-energy mode nearly vanishes in the pentalayer because 90% of the light is transmitted through the stack; the reflectance drops to zero (Fig. 6b). This is remarkable as, e.g., the pentalayer is a 200 nm thick layer that consists of 70% gold. For comparison, the transmittance through a 140 nm thick gold film is 10^{-4}% at 0.8 eV.[37] A similar behavior was reported for three-dimensional gold nanorod crystals where

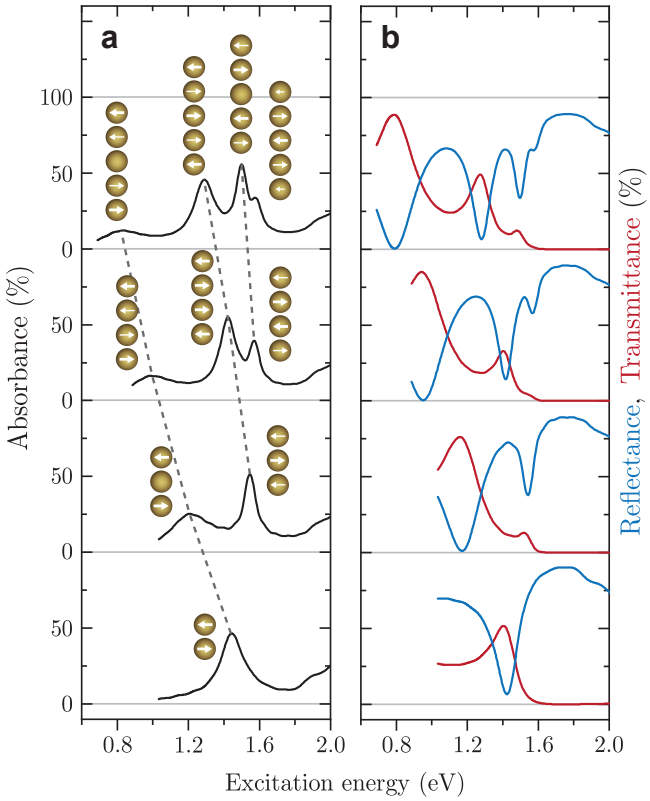

Figure 6: Dark interlayer plasmons in colloidal gold nanoparticle stacks with different layer number; from bilayer (bottom) to pentalayer (top). (a) Absorbance spectra and (b) reflectance and transmittance spectra of the gold nanoparticle layers simulated with FDTD. Hcp stacking, 46 nm sphere diameters, 2 nm gaps and a background medium with a refractive index of $n = 1.4$ were assumed. The plasmonic modes (inset) were assigned via the current distribution inside the nanoparticles; the dipole moments in the particles of each layer are indicated by white arrows. Dashed lines connect similar modes.

light penetrated deep into the crystal and formed standing waves.[38] Fig. 6 shows that the absorptive dark interlayer plasmons transform into such standing waves with increasing layer number. Both the plasmonic modes and the standing wave patterns are accompanied by strong electromagnetic field enhancement between the spheres which can be exploited for sampling large volumes of bioanalytes, e.g., with surface-enhanced Raman scattering.[38–41]

In summary, we demonstrated the direct excitation of a dark plasmons by linearly polarized light, which is generally considered forbidden by selection rules. Because of the finite wavelength of light, antiparallel dipoles are excited in nanoparticles that are stacked along the light path. We demonstrate this concept experimentally using bi- and trilayers

of self-assembled gold nanoparticles. We show by experiment and simulation that particle diameters of 46 nm are sufficient to observe a pronounced (50%) absorption peak in the near infrared that stems from the excitation of dark interlayer plasmons with antiparallel dipoles between the layers. The dark plasmon modes gradually turn into standing waves as the layer number is further increased, which leads to almost perfect transmittance of light through the nanoparticle film. Generally, $n-1$ modes are excited in a film with n nanoparticle layers. Our approach is scalable and easy to implement opening the route to the large-scale exploitation of dark modes in spectroscopy and energy applications.

Methods

FDTD simulations

We used the commercial software package Lumerical FDTD Solutions for the finite-difference time-domain simulations. A total-field scattered-field source was used for simulating the absorption cross-section of the nanodimer. The nanoparticle layers were implemented by constructing the lattice unit cell and using periodic boundary conditions. A plane-wave source was used for excitation. The transmittance T was measured with a monitor behind the nanoparticle layers and the reflectance R by a monitor behind the source. The absorbance A was calculated as $A = 1 - T - R$. The materials were modeled by fitting experimental data of the dielectric function from Johnson and Christy for gold[42] and Palik for silver.[43] We used mesh-override regions of 2 nm for the nanodimer and 0.25 nm for the nanoparticle layers to accurately model the interparticle gaps. The simulated spectra were tested for convergence by changing the mesh sizes. The electrical currents were calculated by averaging the values from seven electrical current monitors that were placed symmetrically in each of the nanoparticle layers. The complex electrical currents were corrected for the phase shift to the incident light that changes with excitation energy.

Synthesis of colloidal gold nanoparticle layers

Materials: Tetrachloroauric(III) acid (≥99.9% trace metals basis), oleylamine (98%), toluene and ethanol (denat.) were purchased from Sigma-Aldrich (USA). Trisodium citrate and diethylene glycol (DEG) were from Merck (Germany). Thiolated polystyrene (PSSH5k: Mn = 5300 g/mol, Mw = 5800 g/mol) was from Polymer Source (Canada). All reagents were analytical grade and used without further treatment. For gold nanoparticle (AuNP) synthesis ultrapure water (18.2 Ω) was used.

AuNP synthesis: Quasispherical citrate stabilized gold nanoparticles (AuNP@Citrate) with a diameter of 46 nm were synthesized based on the seeded-growth protocol.[44] AuNP concentrations were determined based on their absorbance at 450 nm.[45]

Functionalization with polystyrene (PSSH5k): The AuNP@Citrate were functionalized with the PSSH5k ligand based on the phase transfer ligand exchange protocol described recently.[35] PSSH (0.16 mM) and oleylamine (1 mM) in toluene (6 ml) were mixed with the aqueous AuNP@Citrate (6 ml) and ethanol (6 ml) under rapid stirring. The stirring was stopped after 30 minutes and after complete phase separation, the organic phase was carefully extracted and concentrated and purified by centrifugation (12 min × 2,000 g in 1 ml aliquots). The final concentration of the AuNP@PSSH5k was 2.1 nM.

Self-assembly of AuNP@PSSH at the liquid-liquid interface: AuNP@PSSH5k mono- and bilayer films were prepared by self-assembly at the liquid-liquid interface.[35] 300 μL AuNP@PSSH5k solution (2.1 nM) in toluene was pipetted onto 300 μL DEG in a Teflon well. The well was covered with a glass slide and left undisturbed at room temperature until the solvent was evaporated and a golden film had formed. The waiting time was at least 24 h.

Set-up for micro-absorbance measurements

The optical set-up for micro-absorbance measurements is depicted in Fig. 3b. A super-continuum laser (Fianium, SC-400-4) that emits light over a broad spectral range (450 nm

- 2400 nm) was used as a light source. We either reduced the spectral emission to 450 nm - 950 nm by using a spectral splitter (Fianium) or to 700 nm - 1200 nm by using a combination of long- and shortpass filters. The light was guided through a linear polarizer and a beam splitter (Thorlabs, BSW26R) into an inverted microscope (Olympus, IX71). We used a Leica HCX PL Fluotar 100× objective with a numerical aperture (NA) of 0.9 to focus the light onto the sample with a laser power below 100 μW. We confirmed experimentally that the large numerical aperture of the microscope objective has no effect on the measured spectra (see Fig. S7). The gold nanoparticle film was deposited on a TEM grid with a 10 nm amorphous carbon film as support. This amorphous carbon layer does not affect the excitation of the dark interlayer plasmon (Fig. S8). The sample was mounted to a motorized xy-translation stage. The position of the laser spot on the sample was visible through a microscope camera. The transmitted light was collected with an Olympus Mplan FL N BD 100× objective with an NA of 0.9 and guided by a fiber (Ocean Optics, QP600-2-UV-BX for 450 nm - 950 nm and BIF600-VIS-NIR for 700 nm - 1200 nm) to a spectrometer (Avantes, Avaspec 3648). The reflected light was separated from the incoming light with a second beam splitter (Thorlabs, BSW26R) and detected by a spectrometer (same fibers and spectrometer as for the transmitted light).

Transmission-electron microscopy (TEM)

TEM measurements were performed using a Jeol JEM-1011 instrument operating at 100 kV. Samples of self-assembled AuNP@PSSH5k films were carefully skimmed off with carbon coated copper grids held by a tweezer. To increase the probability of bilayer-formation the procedure was repeated with some grids. The grids were then dried on filter paper for at least 24 h. To identify the regions of interest on the grids, optical microscopy images were compared with the same grids under low magnification in the TEM. In this way it was possible to identify the exact mesh and region on the grids where the absorption measurements had been performed.

Acknowledgements

This work was supported by the European Research Council under grant DarkSERS (772108). N.S.M. acknowledges Deutsche Telekom Stiftung for financial support. B.G.M.V. acknowledges the Coordenação de Aperfeiçoamento de Pessoal de Nivel Superior (CAPES) for the financial support under the program PDSE (Grant No. 88881.134611/2016-01) and Dahlem Research School (DRS). E.B.B. acknowledges financial support from CNPq. F.S. was supported by the DFG via the project SCHU 3019/2-1. H.L. acknowledges the German Research Foundation (DFG) for financial support through the Cluster of Excellence CUI. V.O. acknowledges the Evonik Foundation for financial support. P.K. acknowledges the FocusArea NanoScale.

Supporting Information

Simulated absorption cross sections of a dimer that is five times smaller than in Fig. 1b. Simulated absorbance spectrum for a bilayer of silver nanoparticles. Additional experimental and simulated spectra that are not contained in the main text. TEM images of places 1 and 2 in Fig. 4. Simulated absorbance spectra for bilayers of gold nanoparticles with three different interparticle gap sizes. Experimental reflectance spectra of a gold nanoparticle bilayer measured with three microscope objectives with different NA. Simulated reflectance and absorbance spectra of a gold nanoparticle bilayer placed on top of a 10 nm thick amorphous carbon layer. Excitation energy dependence of the electrical current in the tetra- and pentalayer.

References

(1) Kelly, K. L.; Coronado, E.; Zhao, L. L.; Schatz, G. C. The Optical Properties of Metal Nanoparticles: The Influence of Size, Shape, and Dielectric Environment. *J. Phys.*

Chem. B **2003**, *107*, 668–677.

(2) Maier, S. *Plasmonics: Fundamentals and Applications*; Springer US, 2007.

(3) Schuller, J. A.; Barnard, E. S.; Cai, W.; Jun, Y. C.; White, J. S.; Brongersma, M. L. Plasmonics for extreme light concentration and manipulation. *Nat. Mater.* **2010**, *9*, 193–204.

(4) Gramotnev, D. K.; Bozhevolnyi, S. I. Plasmonics beyond the diffraction limit. *Nat. Photonics* **2010**, *4*, 83–91.

(5) Atwater, H. A.; Polman, A. Plasmonics for improved photovoltaic devices. *Nat. Mater.* **2010**, *9*, 205–213.

(6) Moskovits, M. Surface-enhanced spectroscopy. *Rev. Mod. Phys.* **1985**, *57*, 783–826.

(7) Kneipp, K.; Wang, Y.; Kneipp, H.; Perelman, L. T.; Itzkan, I.; Dasari, R. R.; Feld, M. S. Single Molecule Detection Using Surface-Enhanced Raman Scattering (SERS). *Phys. Rev. Lett.* **1997**, *78*, 1667–1670.

(8) Hartstein, A.; Kirtley, J. R.; Tsang, J. C. Enhancement of the Infrared Absorption from Molecular Monolayers with Thin Metal Overlayers. *Phys. Rev. Lett.* **1980**, *45*, 201–204.

(9) Benz, F.; Schmidt, M. K.; Dreismann, A.; Chikkaraddy, R.; Zhang, Y.; Demetriadou, A.; Carnegie, C.; Ohadi, H.; de Nijs, B.; Esteban, R.; Aizpurua, J.; Baumberg, J. J. Single-molecule optomechanics in "picocavities". *Science* **2016**, *354*, 726–729.

(10) Sönnichsen, C.; Franzl, T.; Wilk, T.; von Plessen, G.; Feldmann, J.; Wilson, O.; Mulvaney, P. Drastic Reduction of Plasmon Damping in Gold Nanorods. *Phys. Rev. Lett.* **2002**, *88*, 077402.

(11) Mayer, K. M.; Hafner, J. H. Localized Surface Plasmon Resonance Sensors. *Chem. Rev.* **2011**, *111*, 3828–3857.

(12) Gramotnev, D. K.; Bozhevolnyi, S. I. Tunable subradiant lattice plasmons by out-of-plane dipolar interactions. *Nat. Nanotechnol.* **2011**, *6*, 423–427.

(13) Panaro, S.; Nazir, A.; Liberale, C.; Das, G.; Wang, H.; De Angelis, F.; Proietti Zaccaria, R.; Di Fabrizio, E.; Toma, A. Dark to Bright Mode Conversion on Dipolar Nanoantennas: A Symmetry-Breaking Approach. *ACS Photonics* **2014**, *1*, 310–314.

(14) Humphrey, A. D.; Meinzer, N.; Starkey, T. A.; Barnes, W. L. Surface Lattice Resonances in Plasmonic Arrays of Asymmetric Disc Dimers. *ACS Photonics* **2016**, *3*, 634–639.

(15) Chuntonov, L.; Haran, G. Trimeric Plasmonic Molecules: The Role of Symmetry. *Nano Lett.* **2011**, *11*, 2440–2445.

(16) Liu, M.; Lee, T.-W.; Gray, S. K.; Guyot-Sionnest, P.; Pelton, M. Excitation of Dark Plasmons in Metal Nanoparticles by a Localized Emitter. *Phys. Rev. Lett.* **2009**, *102*, 107401.

(17) Peyskens, F.; Subramanian, A. Z.; Neutens, P.; Dhakal, A.; Dorpe, P. V.; Thomas, N. L.; Baets, R. Bright and dark plasmon resonances of nanoplasmonic antennas evanescently coupled with a silicon nitride waveguide. *Opt. Express* **2015**, *23*, 3088–3101.

(18) Pakizeh, T.; Abrishamian, M. S.; Granpayeh, N.; Dmitriev, A.; Käll, M. Magnetic-field enhancement in gold nanosandwiches. *Opt. Express* **2006**, *14*, 8240–8246.

(19) Verre, R.; Yang, Z. J.; Shegai, T.; Käll, M. Optical Magnetism and Plasmonic Fano Resonances in Metal-Insulator-Metal Oligomers. *Nano Lett.* **2015**, *15*, 1952–1958.

(20) Sancho-Parramon, J.; Bosch, S. Dark Modes and Fano Resonances in Plasmonic Clusters Excited by Cylindrical Vector Beams. *ACS Nano* **2012**, *6*, 8415–8423.

(21) Gómez, D. E.; Teo, Z. Q.; Altissimo, M.; Davis, T. J.; Earl, S.; Roberts, A. The Dark Side of Plasmonics. *Nano Lett.* **2013**, *13*, 3722–3728.

(22) Sakai, K.; Nomura, K.; Yamamoto, T.; Sasaki, K. Excitation of Multipole Plasmons by Optical Vortex Beams. *Sci. Rep.* **2015**, *5*.

(23) Luk'yanchuk, B.; Zheludev, N. I.; Maier, S. A.; Halas, N. J.; Nordlander, P.; Giessen, H.; Chong, C. T. The Fano resonance in plasmonic nanostructures and metamaterials. *Nat. Mater.* **2010**, *9*, 707–715.

(24) Prodan, E.; Radloff, C.; Halas, N. J.; Nordlander, P. A Hybridization Model for the Plasmon Response of Complex Nanostructures. *Science* **2003**, *302*, 419–422.

(25) Chu, M.-W.; Myroshnychenko, V.; Chen, C. H.; Deng, J.-P.; Mou, C.-Y.; García de Abajo, F. J. Probing Bright and Dark Surface-Plasmon Modes in Individual and Coupled Noble Metal Nanoparticles Using an Electron Beam. *Nano Lett.* **2009**, *9*, 399–404.

(26) Nordlander, P.; Oubre, C.; Prodan, E.; Li, K.; Stockman, M. I. Plasmon Hybridization in Nanoparticle Dimers. *Nano Lett.* **2004**, *4*, 899–903.

(27) Jorio, A.; Mueller, N. S.; Reich, S. Symmetry-derived selection rules for plasmon-enhanced Raman scattering. *Phys. Rev. B* **2017**, *95*, 155409.

(28) Hohenester, U.; Trügler, A. MNPBEM: A Matlab toolbox for the simulation of plasmonic nanoparticles. *Comput. Phys. Commun.* **2012**, *183*, 370 – 381.

(29) Chang, Y.-C.; Wang, S.-M.; Chung, H.-C.; Tseng, C.-B.; Chang, S.-H. Observation of Absorption-Dominated Bonding Dark Plasmon Mode from Metal-Insulator-Metal Nanodisk Arrays Fabricated by Nanospherical-Lens Lithography. *ACS Nano* **2012**, *6*, 3390–3396.

(30) Dmitriev, A.; Pakizeh, T.; Käll, M.; Sutherland, D. S. Gold-Silica-Gold Nanosandwiches: Tunable Bimodal Plasmonic Resonators. *Small* **2007**, *3*, 294–299.

(31) Frederiksen, M.; Bochenkov, V. E.; Ogaki, R.; Sutherland, D. S. Onset of Bonding

Plasmon Hybridization Preceded by Gap Modes in Dielectric Splitting of Metal Disks. *Nano Lett.* **2013**, *13*, 6033–6039.

(32) Ogier, R.; Shao, L.; Svedendahl, M.; Käll, M. Continuous-Gradient Plasmonic Nanostructures Fabricated by Evaporation on a Partially Exposed Rotating Substrate. *Adv. Mater.* **2016**, *28*, 4658–4664.

(33) Pinchuk, A.; von Plessen, G.; Kreibig, U. Influence of interband electronic transitions on the optical absorption in metallic nanoparticles. *J. Phys. D: Appl. Phys.* **2004**, *37*, 3133.

(34) Ullrich, S.; Scheeler, S. P.; Pacholski, C.; Spatz, J. P.; Kudera, S. Formation of Large 2D Arrays of Shape-Controlled Colloidal Nanoparticles at Variable Interparticle Distances. *Part. Part. Syst. Charact.* **2012**, *30*, 102–108.

(35) Schulz, F.; Tober, S.; Lange, H. Size-Dependent Phase Transfer Functionalization of Gold Nanoparticles To Promote Well-Ordered Self-Assembly. *Langmuir* **2017**, *33*, 14437–14444.

(36) Zhang, X. M.; Xiao, J. J.; Zhang, Q.; Li, L. M.; Yao, Y. Plasmonic TM-like cavity modes and the hybridization in multilayer metal-dielectric nanoantenna. *Opt. Express* **2015**, *23*, 16122–16132.

(37) Lodenquai, J. F. Electromagnetic wave propagation in media with complex refractive indices and transmission through absorbing films. *Am. J. Phys.* **1991**, *59*, 248–254.

(38) Solís, D. M.; Taboada, J. M.; Obelleiro, F.; Liz-Marzán, L. M.; García de Abajo, F. J. Toward Ultimate Nanoplasmonics Modeling. *ACS Nano* **2014**, *8*, 7559–7570.

(39) Hamon, C.; Novikov, S. M.; Scarabelli, L.; Solís, D. M.; Altantzis, T.; Bals, S.; Taboada, J. M.; Obelleiro, F.; Liz-Marzán, L. M. Collective Plasmonic Properties in Few-Layer Gold Nanorod Supercrystals. *ACS Photonics* **2015**, *2*, 1482–1488.

(40) Matricardi, C.; Hanske, C.; Garcia-Pomar, J. L.; Langer, J.; Mihi, A.; Liz-Marzán, L. M. Gold Nanoparticle Plasmonic Superlattices as Surface-Enhanced Raman Spectroscopy Substrates. *ACS Nano* **2018**, *12*, 8531–8539.

(41) Wei, W.; Wang, Y.; Ji, J.; Zuo, S.; Li, W.; Bai, F.; Fan, H. Fabrication of Large-Area Arrays of Vertically Aligned Gold Nanorods. *Nano Lett.* **2018**, *18*, 4467–4472.

(42) Johnson, P. B.; Christy, R. W. Optical Constants of the Noble Metals. *Phys. Rev. B* **1972**, *6*, 4370–4379.

(43) Palik, E. *Handbook of Optical Constants of Solids*; Academic Press handbook series Bd. 1; Academic Press, 1985.

(44) Bastús, N. G.; Comenge, J.; Puntes, V. Kinetically Controlled Seeded Growth Synthesis of Citrate-Stabilized Gold Nanoparticles of up to 200 nm: Size Focusing versus Ostwald Ripening. *Langmuir* **2011**, *27*, 11098–11105.

(45) Haiss, W.; Thanh, N. T. K.; Aveyard, J.; Fernig, D. G. Determination of Size and Concentration of Gold Nanoparticles from UV-Vis Spectra. *Anal. Chem.* **2007**, *79*, 4215–4221.

Graphical TOC Entry